

Active dilation of penetrating arterioles restores red blood cell flux to penumbral neocortex after focal stroke

Andy Y Shih¹, Beth Friedman², Patrick J Drew¹, Philbert S Tsai¹, Patrick D Lyden^{2,3} and David Kleinfeld^{1,3}

¹Department of Physics, University of California at San Diego, La Jolla, California, USA; ²Department of Neuroscience, University of California at San Diego, La Jolla, California, USA; ³Graduate Program in Neurosciences, University of California at San Diego, La Jolla, California, USA

Pial arterioles actively change diameter to regulate blood flow to the cortex. However, it is unclear whether arteriole reactivity and its homeostatic role of conserving red blood cell (RBC) flux remains intact after a transient period of ischemia. To examine this issue, we measured vasodynamics in pial arteriole networks that overlie the stroke penumbra during transient middle cerebral artery occlusion in rat. *In vivo* two-photon laser-scanning microscopy was used to obtain direct and repeated measurements of RBC velocity and lumen diameter of individual arterioles, from which the flux of RBCs was calculated. We observed that occlusion altered surface arteriole flow patterns in a manner that ensured undisturbed flow to penetrating arterioles throughout the imaging field. Small-diameter arterioles (<23 μm), which included 88% of all penetrating arterioles, exhibited robust vasodilation over a 90-min occlusion period. Critically, persistent vasodilation compensated for an incomplete recovery of RBC velocity during reperfusion to enable a complete restoration of postischemic RBC flux. Further, histologic examination of tissue hypoxia suggested re-oxygenation through all cortical layers of the penumbra. These findings indicate that selective reactivity of small pial arterioles is preserved in the stroke penumbra and acts to conserve RBC flux during reperfusion.

Journal of Cerebral Blood Flow & Metabolism advance online publication, 28 January 2009; doi:10.1038/jcbfm.2008.166

Keywords: homeostasis; ischemia; rodent; two-photon microscopy; vasculature

Introduction

The *in vivo* examination of blood flow in single arterioles has been a valuable approach to studying vascular function under normal and pathologic conditions. In rats, the perfusion of each cubic millimeter of neocortex is strictly regulated by 10 or more penetrating arterioles (Nishimura *et al*, 2007), which are in turn supplied by a highly interconnected plexus of surface arterioles with heterogeneous flow profiles (Bar, 1980; Schaffer

et al, 2006). The vascular response to change in neuronal input (Devor *et al*, 2007, 2008) or to the disruption of blood flow (Kontos *et al*, 1978) involves populations of arterioles that react differently based on their size and location within the network. Thus, examination of blood flow in the level of individual vessels is necessary to characterize these responses.

Red blood cell (RBC) velocity in pial arterioles is, on average, an order of magnitude faster than in capillaries. Using confocal or two-photon laser-scanning microscopy, RBC velocity is tracked in individual arterioles using high-speed line scans (Dirnagl *et al*, 1992; Kleinfeld *et al*, 1998), and vessel diameters are concurrently determined from planar image stacks. These two measurements are then combined to determine the volume flux of RBCs, which provides a complete description of blood flow in each vessel (Ngai and Winn, 1996; Rovainen *et al*, 1993; Schaffer *et al*, 2006).

We apply this technique to examine the important issue of whether homeostatic regulation of RBC flux is preserved in the acutely recovering stroke

Correspondence: Dr D Kleinfeld, Department of Physics, University of California at San Diego, 9500 Gilman Drive, La Jolla, CA 92093-0374, USA.

E-mail: dk@physics.ucsd.edu

This work was funded by the Canadian Institutes of Health Research, the National Institutes of Health (NCRR, NIA, NIBIB, and NINDS), the National Science Foundation, and the Veterans Medical Research Foundation.

Received 9 July 2008; revised 9 December 2008; accepted 12 December 2008

penumbra (Iadecola, 1998). The preservation of cerebrovascular reactivity is critical for buffering variations in postischemic blood flow (Paulson *et al*, 1990), and the loss of this function in humans has been linked to the recurrence of stroke and to poor recovery from stroke (Marshall, 2004). Severe ischemia in the focal stroke core can compromise the myogenic response to changes in arteriole pressure (Cipolla *et al*, 2001). However, less is known about the state of arterioles in the stroke penumbra, where residual blood flow may be sufficient to preserve vascular function and improve tissue recovery after reperfusion (Dirnagl and Pulsinelli, 1990; Iadecola, 1998). This includes the effect of stroke on penetrating arteriole reactivity, which constitutes ~40% of the cerebrovascular resistance for blood flow (Cipolla *et al*, 2004; Heistad and Kontos, 1983).

We measured the vasodynamics of flow in pial arterioles across the stroke penumbra in the parietal cortex during 90 mins of transient middle cerebral artery occlusion (tMCAo). We ask the following questions: (i) How does the pattern of RBC flow in the pial arteriole network change in response to MCA occlusion, and what is the role of these flow changes? (ii) Does the measurement of RBC velocity or lumen diameter alone accurately predict RBC flux during stroke? (iii) Is compensatory arteriole reactivity intact after stroke, and are penetrating arterioles, as a population, able to maintain normal levels of flux? Importantly, these questions are not accessible to laser Doppler flowmetry (LDF), which records from multiple vessels and, in practice, is insensitive to the relatively high flow rates in pial vessels (Barfod *et al*, 1997). Rather, we make use of *in vivo* two-photon laser-scanning microscopy to obtain systematic and repeated measurements of RBC velocity and lumen diameter in individual surface and penetrating arterioles.

Materials and methods

Animal Models and Surgery

In total, 57 male Sprague–Dawley rats were used in this study (Charles River, Hollister, CA, USA), ranging in mass from 270 to 310 g. Thirteen animals were imaged during tMCAo using the Koizumi method, that is, ligation of the ipsilateral common carotid artery (CCA) during reperfusion (Koizumi *et al*, 1986); 4 for tMCAo using the Longa method, that is, the ipsilateral CCA is intact during reperfusion (Longa *et al*, 1989); 7 for sham tMCAo controls, that is, ipsilateral CCA ligation and partial filament insertion (Supplementary Figure 2); 6 for Window-only controls, that is, cranial window but no vascular manipulation (Supplementary Figure 3); 4 for hypercapnic treatment to control for large surface arteriole dilation; 12 for pimonidazole studies using the Koizumi method; and 11 for LDF studies. Anesthesia was maintained with 1 to 2% (v/v) isoflurane (Baxter Healthcare, Deerfield, IL, USA) in 30% oxygen and 70% nitrous oxide. As isoflurane is a vasodilator that can affect cerebral autoregulation (Eger,

1981), the Window-only group controlled for the effects of anesthesia over time (Supplementary Figure 3). Atropine (American Regent, Shirley, NY, USA), 0.05 mg per kg body weight intraperitoneal, and lidocaine (Hospira Inc., Lake Forest, IL, USA), 2% (v/v) subcutaneous, were administered at the start of surgery. Body temperature was maintained at 37°C with a feedback-regulated heat pad (50-7053-F; Harvard, Holliston, MA, USA). Heart rate and blood oxygen saturation were continuously monitored using a pulse oximeter (8600V; Nonin, Plymouth, MN, USA). Cranial windows, 4 × 4 mm in size and centered at 4.5 mm medial–lateral and –3.0 mm anterior–posterior, were constructed, as described earlier (Kleinfeld *et al*, 2008). The left femoral artery was catheterized with polyethylene 50 tubing (BD diagnostics, Sparks, MD, USA) connected to a stopcock and a 10-mL syringe filled with heparin saline (20 units per mL, Baxter Healthcare). Arterial blood was sampled from the catheter for blood gas measurement (RapidLab 248; Bayer, Norwood, MA, USA) during each of three imaging periods, that is, baseline, occlusion, and reperfusion. Blood pressure was measured with the tail cuff method (XBP-1000; Kent Scientific, Torrington, CT, USA) once during each imaging period. Intraperitoneal injections of 5% (w/v) glucose in 1 mL saline were given every 2 h for re-hydration.

Transient middle cerebral artery re-occlusion was induced using the intraluminal filament method. Ischemia was maintained for 90 mins and followed by 90 mins of reperfusion. We examined two variations of the model and exploited their differences in postischemic blood flow. In the majority of the experiments, the CCA was permanently ligated to generate an incomplete reperfusion (Koizumi *et al*, 1986). In a control study, we left the CCA intact, which generated a transient hyperemia during the reperfusion period (Longa *et al*, 1989). In all cases, the filament placement was guided with LDF measurements through the cranial window. Animals that exhibited subarachnoid hemorrhage were excluded from the study.

The penumbra was defined by the amount of residual blood flow during occlusion, typically ranging within 25% to 50% of baseline flow values, measured either using LDF or averaging arteriole flux measurements from the cranial window. This level of blood flow in the penumbra is a generally accepted range (Lipton, 1999) and is contrasted to flow in the ischemic core, which can be lower than 20% of baseline.

Two-Photon Microscopy

Images were collected using a two-photon laser scanning microscope of local design (Tsai *et al*, 2003; Tsai *et al*, 2002), which was controlled by MPscope software (Nguyen *et al*, 2006). The blood serum was labeled using 0.3 mL of 2 MDa fluorescein dextran (FD2000S; Sigma, St Louis, MO, USA) prepared at a concentration of 5% (w/v) in saline, and delivered through the femoral artery catheter, with 0.1 mL supplements as required (Schaffer *et al*, 2006). A 0.3 numerical aperture (NA), ×10 magnification water-dipping objective (Zeiss, Thornwood, NY, USA) was used to collect a large-scale map to aid navigation through the

cortical vasculature, whereas a 0.8-NA, $\times 40$ magnification water-dipping objective (Olympus, Center Valley, PA, USA) was used to obtain high-resolution line scan and planar data. The line scans were collected along the centerline of each vessel over a length of 70 pixels, spanning 7 to 76 μm , at a scan rate of 1.6 kHz/line. Red blood cell velocity was determined from the slope of the line-scan streaks using a method based on singular value decomposition (Kleinfeld *et al*, 1998). For each vessel, we reported the average velocity over a 1.5-s period. Planar image stacks, 256×256 pixels, were acquired to establish the diameter of the vessel. Our analysis was limited to arterioles smaller than 60 μm in diameter as a result of technical constraints. A further limitation was that penetrating arterioles could only be measured if a portion of the vessel was parallel to the cortical surface before diving perpendicularly. In a survey of 154 penetrating arterioles across 11 rats, 17% were not measurable as a result of this limitation.

During analysis of surface arterioles, a 23- μm breakpoint was used to divide the vessels into small- and large-diameter categories. This number corresponded to the intersection between normalized histograms for penetrating arteriole ($n=215$) and surface arteriole ($n=271$) diameters at baseline, and by maximum likelihood, was the natural point to divide the data. Further, 23 μm was the median diameter for measured surface arterioles.

Flux Quantification

Under the assumption that the flow in the vessels is laminar, RBC velocity and lumen diameter collected from a single vessel can be used to define the average volume flux, \vec{F} , by:

$$\vec{F} = \langle \vec{v} \rangle A = \frac{\pi}{8} \vec{v}(0) d^2 \quad (1)$$

where $\langle \vec{v} \rangle$ is the average RBC velocity, A the cross-sectional area of the vessel lumen, $\vec{v}(0)$ the RBC velocity along the central axis of the vessel, and d the lumen diameter. Our sign convention is that positive velocity points in the direction of flow prior to the occlusion. The constraint of constant flux implies that the change in diameter, Δd , that is required to offset a change in speed, that is, $\Delta \vec{v}(0)$, is given by

$$\frac{\Delta d}{d} = \sqrt{\frac{1}{1 + \Delta \vec{v}(0)/\vec{v}(0)}} - 1 \xrightarrow{\Delta \vec{v} \rightarrow 0} -\frac{1}{2} \frac{\Delta \vec{v}(0)}{\vec{v}(0)} \quad (2)$$

A decrease in $\vec{v}(0)$, that is, $\Delta \vec{v}(0) < 0$, yields an increase in d , that is, $\Delta d > 0$.

Vascular Casting

A fluorescent agarose gel was formulated from 0.42% (w/v) 2MDa fluorescein dextran and 1% (w/v) low gelling temperature agarose (A4018; Sigma) in phosphate-buffered saline (PBS), mixed at 60°C, and maintained at 40°C before use (Tsai, 2004). Cerebral blood vessels were dilated by administration of 5% CO₂ and 95% O₂ with 2% isoflurane through a nose cone for 15 mins to facilitate perfusion of the gel. Animals were perfused transcidentally through the left ventricle with 100 mL of PBS, 100 mL of 4% paraformaldehyde,

another 50 mL of PBS to wash out residual fixative. Gel (50 mL) was then steadily injected into the ventricle using a syringe at a rate of ~ 2 mL per sec. The gel was rapidly solidified *in situ* by placing the animal in an ice bath. The brain was carefully extracted to avoid damage to pial vessels. The cortex of the ischemic hemisphere was removed and flattened between two glass slides separated by a distance of 3 mm for wide-field fluorescence microscopy (Axioplan 2; Zeiss). The arteriole network, including the region imaged *in vivo*, was traced from overlapping images taken with a 0.5-NA $\times 10$ magnification air objective (Zeiss).

Pimonidazole Immunohistochemistry

Pimonidazole hydrochloride (Hypoxyprobe™; <http://www.hypoxyprobe.com>) is a sensitive method for detecting even small volumes of tissue hypoxia, that is, < 10 mmHg tissue oxygen, compared with ~ 30 mmHg under normoxic conditions (Nishimura *et al*, 2006; Takasawa *et al*, 2008). Pimonidazole was injected through the femoral artery catheter at a concentration of 60 mg per kg body weight. For immunostaining, 50- μm -thick frozen sections were treated for 10 mins with 3% (v/v) H₂O₂, and incubated for 72 h at room temperature in an anti-Hypoxyprobe antibody diluted 10³ times in PBS containing 10% (v/v) of normal goat serum (Vector Laboratories, Burlingame, CA, USA), 2% (v/v) of Triton X-100 (Sigma), and 0.2% (v/v) of sodium azide (Sigma). Bound antibody was visualized with the Vectastain ABC kit and diaminobenzadine peroxidase substrate kit (both from Vector Laboratories), and brain sections were photographed using a MacroView microscope (MVX10; Zeiss). Pimonidazole staining was quantified from brain sections, originating from bregma -3.0 mm anterior–posterior, by first determining the normalized intensity histogram for staining in both ischemic (ipsilateral) and nonischemic (contralateral) cortices. A threshold, set to include the largest 90% of pixel values from the nonischemic side, was then used to isolate stained regions on the ischemic side, which was presented as a percentage of the total cortical area.

Laser Doppler Flowmetry

Flowmetry measurements were performed with a MoorLab unit (Moor Instruments, Millwey, Axminster, Devon, UK; $\lambda_o = 780$ nm and $f_{\text{cut}} = 15$ kHz low-pass filtered, to give a maximum measurable speed of $\lambda_o f_{\text{cut}}/2 = 6$ mm/sec), fitted with an MP1-V2 probe tip that was held in place with a custom adaptor over the cranial window or thinned skull. The LDF ‘flux’ output, a measure of average RBC velocity multiplied by the intensity of the reflected signal, was collected at a sampling rate of 40 Hz using WinEDR software (http://spider.science.strath.ac.uk/sipbs/software_ses.htm), and averaged over 60-sec intervals.

Statistics

Data are presented as mean \pm s.e.m. We used the nonparametric Wilcoxon signed rank test unless otherwise stated, as the *in vivo* imaging data were not always normally distributed.

In Figure 4, differences between experimental means and a theoretical line of conserved flux were tested with a two-tailed one-sample *t*-test. In Figure 6, differences between the pimonidazole-stained cortical area were analyzed with an unpaired *t*-test. In Figure 7, vasodynamic changes between imaging periods were analyzed using a two-tailed paired *t*-test.

Results

Pial Arteriole Vasodynamics under Basal Conditions

We obtained an overview of RBC flux from surface and penetrating arterioles through a cranial window

in the anesthetized rats (Figures 1A to 1C). Line scans were used to measure the centerline velocity (maximal velocity) of RBCs in individual arterioles, denoted as $\vec{v}(0)$, followed immediately by the collection of an image stack to measure vessel diameter, d (Figures 1D and 1E). A random sampling of surface arterioles at baseline yielded RBC velocities that ranged from 1.4 to 34 mm/sec in vessels with diameters between 5 and 60 μm (Figure 1F). The range of velocities in penetrating arterioles was similar, 0.7 to 35 mm/sec, but all vessels were 30 μm or less in diameter (Figure 1G). Velocities were significantly correlated with diameter for both

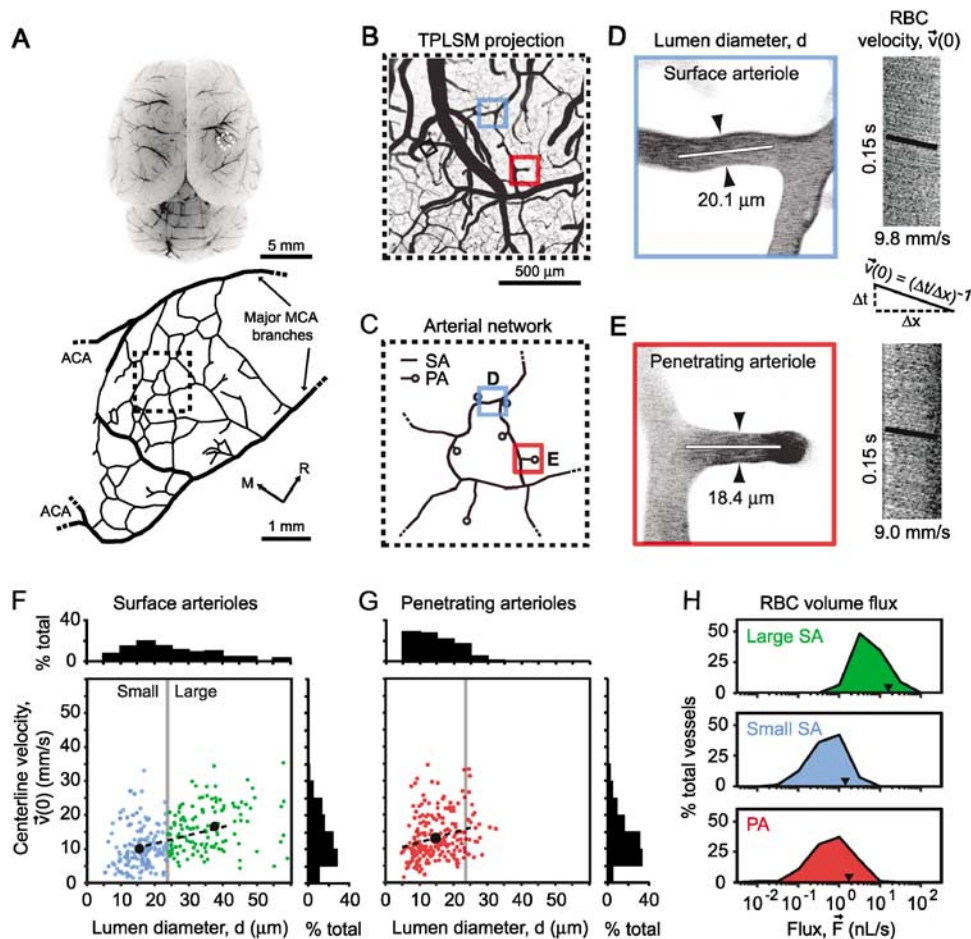


Figure 1 Vascular parameters of individual pial arterioles under basal conditions. **(A)** The location of the imaged region over the right dorsolateral cortex is marked (dashed square). Below, a tracing of the MCA network, derived from the vascular casting method, shows the imaged region (dashed square) relative to major distal MCA branches (thick black lines) and detailed interconnecting loop structures (thin black lines). M, medial; R, rostral. **(B)** A flattened 3-D image stack collected from the cranial window, i.e., maximal Z axis projection (300 μm depth, 5 μm steps). All TPLSM (two-photon laser-scanning microscopy) images were inverted for improved contrast of the vasculature. **(C)** Arteriole tracing of the imaged region, which reveals surface arterioles (SA) and penetrating arterioles (PA) that were randomly sampled. The analysis of a typical surface arteriole (blue square) and penetrating arteriole (red square) is shown. **(D and E)** Lumen diameter, d , was measured from maximal projections of planar 3-D image stacks (distance between arrowheads). Line scans were repeatedly collected from the arteriole centerline axis (white line) and stacked sequentially to form a space-time image. The streaks within the line-scan image represent non-fluorescent RBC moving through a fluorescent background, with the x axis representing the distance traveled by the RBCs, x , and the y axis representing time, t . Centerline RBC velocity, $\vec{v}(0)$, was then calculated from the inverse of the slope of the RBC streaks, as shown in the equation. **(F and G)** Centerline velocity of RBCs from three categories of arterioles: large surface arterioles, small surface arterioles, and penetrating arterioles, plotted as a function of lumen diameter. The mean velocity and diameter of each arteriole category (black circle) and linear fit (dotted line) are shown. **(H)** Histogram of the range of RBC fluxes, and average flux (arrowhead), for each arteriole category.

surface arterioles, $r=0.49$ ($P < 10^{-4}$), and penetrating arterioles, $r=0.26$ ($P < 10^{-4}$). To emphasize size-based differences in our subsequent analyses, we separated the arterioles into three categories, namely large surface arterioles ($d > 23 \mu\text{m}$, that is, diameters greater than the median diameter of surface arterioles), small surface arterioles ($d < 23 \mu\text{m}$), and penetrating arterioles. The flux of RBCs (Equation (1)) in large surface arterioles ranged from 0.3 to 100 nL/sec, whereas flux in small surface arterioles and penetrating arterioles were, on average, an order of magnitude lower, typically between 0.01 and 10 nL/sec (Figure 1H).

Pial Arteriole Vasodynamics in Response to Transient Middle Cerebral Artery Occlusion

We used the intraluminal filament model to transiently occlude the MCA origin for 90 mins followed by 90 mins of reperfusion (Koizumi *et al*, 1986). We first considered stroke-induced change in RBC flow direction within the pial network, followed by quantitative near-simultaneous measurements of RBC velocity and lumen diameter. We then combined these two measurements to assess volume flux of RBCs. Physiologic parameters including blood gas, blood pressure, and core temperature were within normal limits throughout the imaging sessions

(Supplementary Table 1). Unnormalized values for all measured vasodynamic parameters are provided in Supplementary Figure 1.

Middle Cerebral Artery Occlusion Causes Red Blood Cell Flow Reversal in Surface Arterioles but not in Penetrating Arterioles

Reversal in the flow direction or stalling in the movement of RBCs was observed in 12% of the total measured surface arterioles during occlusion. These changes typically occurred in three network patterns: (i) small surface arteriole loops spanning $\sim 500 \mu\text{m}^2$ of the cortical surface area (7% of total surface arterioles) (Figure 2A); (ii) direct arteriole connections between MCA and anterior cerebral artery (ACA) perfusion sources (3%) (Figure 2B) (Schaffer *et al*, 2006); and (iii) anastomoses that balanced blood flow between major branches of the MCA (2%) (Figure 2C). We used postmortem analysis of fluorescent vascular casts to further evaluate the connectivity of vessels beyond the imaged region (Figure 1A). In general, 72% of the examined surface arterioles were located within loops or directly linked to collaterals of the ACA. Reperfusion resolved nearly all reversals and stalls in the surface network. In contrast to the case for surface arterioles, flow in the penetrating arterioles neither reversed

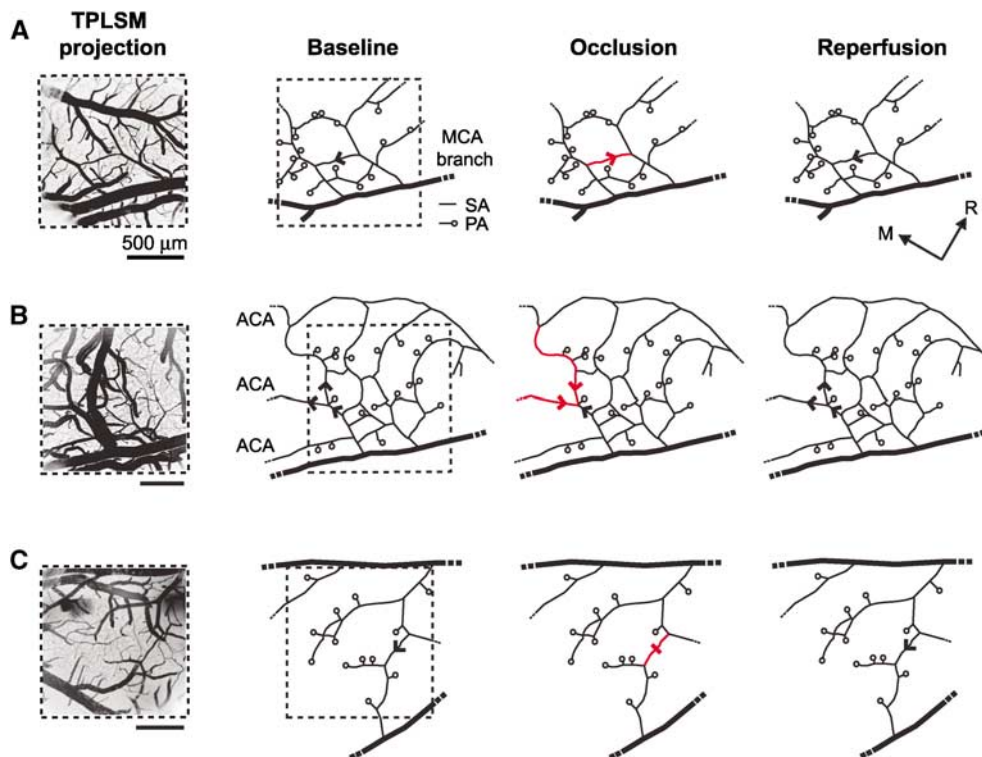


Figure 2 Shifting of RBC flow patterns in surface arteriole networks during tMCAo. Arrowheads indicate the direction of blood flow in arteriole networks. Flow reversals (red dash) and a stall (red dash) caused by MCA occlusion are highlighted. (A) Representative example of flow reversal within a small arteriole loop. (B) Flow reversal in large arterioles that formed anastomoses between ACA and MCA territories. (C) Stalling of flow in arteriole that connected perfusion between two major MCA branches.

nor stalled during the occlusion, but rather responded homogeneously to the overall decrease in blood flow. As a guiding hypothesis, this suggests that flow irregularities in the surface network act to maintain uninterrupted flow to penetrating arterioles during occlusion.

Change in Red Blood Cell Velocity and Lumen Diameter during Transient Middle Cerebral Artery Occlusion

The Koizumi method of tMCAo involves permanent ligation of the ipsilateral CCA, which generates an incomplete recovery of blood flow during reperfusion, as detected by LDF (Figure 3A) (Koizumi *et al*, 1986). We exploited this feature of the model to determine whether arteriole reactivity remains intact and capable of compensating for incomplete reperfusion.

Overall, the RBC velocity across each class of arterioles decreased to ~30% of the baseline levels during occlusion (Figure 3C, left panel); this degree of ischemia falls within a range defined as penumbral flow (Lipton, 1999). After 90 mins of occlusion, the filament was retracted to initiate reperfusion. In 11 of 13 experiments, reperfusion was accompanied by a substantial recovery of RBC velocities toward their baseline values (Figure 3C, right panel). Nonetheless, the velocities across all arterioles recovered to only ~70% of their baseline levels, similar to LDF measurements (Figure 3A) (data include 65 large surface arterioles, 56 small surface arterioles, and 75 penetrating arterioles over 11 animals).

In two cases of tMCAo, flow values were sufficiently low to be categorized as stroke core, that is, flow decreased to 17% and 13% of baseline levels. Recovery of RBC velocities was poor in these cases, returning to only 35% and 38% of baseline levels upon reperfusion, respectively, in contrast to ~70% for the main cluster of tMCAo cases. As these severely ischemic cases represented a small proportion of the total animals, they were removed as outliers in subsequent analyses of the data.

Lumen diameter of small surface arterioles and penetrating arterioles increased by an average of ~20% over baseline levels (Figures 3B, left and center panel, and 3D, left panel) during occlusion. This vasodilation persisted into the reperfusion period (Figures 3B, right panel, and 3D, right panel), and was observed as late as 90 mins after de-occlusion, indicating a prolonged contribution to postischemic blood flow (data not shown). In contrast, the diameter of large surface arterioles exhibited both dilation and constriction, but on average did not change significantly from baseline at any stage during tMCAo (Figure 3D). However, large surface arterioles dilated uniformly in response to hypercapnia, which verifies that these vessels were

not already maximally dilated by generation of the cranial window (Supplementary Materials).

Vasodilation Inversely Tracks Red Blood Cell Velocity to Conserve Flux after Ischemia

The above results show a net increase in the diameter of small surface arterioles and penetrating arterioles concomitant with the net decrease in the RBC velocity during both periods of occlusion and reperfusion. Does the change in diameter compensate for decrease in velocity to conserve RBC flux (Equation (2))? During occlusion, the dilation was insufficient to maintain baseline levels of RBC flux through penetrating arterioles and the mean change corresponded to a significant net drop in flux ($P < 0.001$) (Figure 4A; red box, mean ± 2 s.e.m., lies far from the theoretical line for conserved flux). In contrast, when reperfusion was initiated, the mean arteriole diameter remained dilated such that baseline levels of flux were achieved despite incomplete recovery of RBC velocity. This central result indicates that persistent vasodilation during reperfusion was an enabling factor for the complete recovery of flux to baseline levels in small arterioles (Figure 4B; red box, mean ± 2 s.e.m., lies atop theoretical line for conserved flux).

To control for the effects of generating a cranial window, we also imaged a Window control group, that is, cranial window without vascular manipulation. This group showed no significant change in either diameter or velocity through two rounds of imaging, which corresponded to the same time schedule as occlusion and reperfusion in the tMCAo group, and thus no significant deviation from conserved flux was observed for the mean response (Figures 4C and 4D) (Supplementary Figure 3). The Window control group also revealed an inherent variability in the measured parameters in individual vessels over time. Although the mean response of vessel populations collected over many animals indicated a clear association with the line for conserved flux, vasodynamic changes did not necessarily conform to this theory at the level of individual vessels.

To further examine the relationship between RBC flux and vessel diameter, and to verify the accuracy of our measurements, we calculated flux for all vessels in the tMCAo experiments (Equation (1)). When normalized flux was plotted as a function of lumen diameter (Figure 5A), a clear preferential recovery of small surface arterioles and penetrating arterioles, as opposed to large surface arterioles, was observed during the reperfusion period. This is consistent with specific dilation of small-diameter arterioles shown in Figure 3D.

Our claims depend on an absence of systematic errors in the determination of RBC flux. As a control, we checked whether the measured input into a small

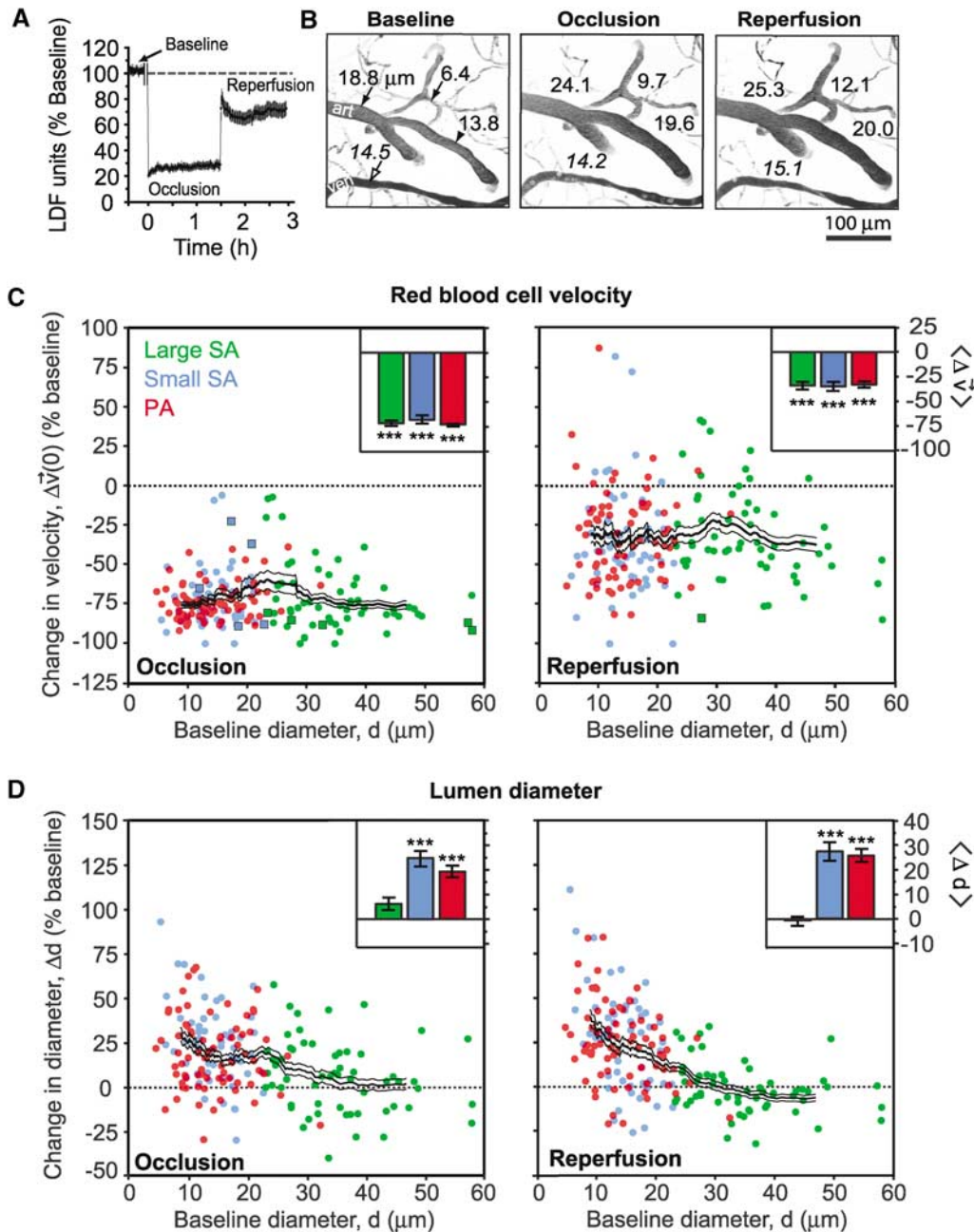


Figure 3 Change in RBC velocity and lumen diameter during tMCAo. **(A)** Relative changes in LDF signal from the cranial window in the Koizumi model of tMCAo (Koizumi *et al*, 1986). Laser Doppler flowmetry data represent mean \pm s.e.m. from $n = 8$ animals. An approximately 10-min period during the filament insertion was omitted from the trace. **(B)** Robust stroke-induced vasodilation in a network of small surface arterioles and penetrating arterioles. The images are maximal projections of $100 \mu\text{m}$ deep image stacks with $5 \mu\text{m}$ steps. Lumen diameters, in μm , of surface arterioles (filled arrows), a penetrating arteriole (filled arrowhead), and a venule (open arrow) are shown at each stage of tMCAo. **(C)** Change in RBC velocity during occlusion and reperfusion plotted as a function of baseline diameter. Square data points represent arterioles with reversed flow with respect to baseline. **(D)** Change in lumen diameter during occlusion and reperfusion plotted as a function of baseline diameter. For panels C and D, a running average \pm s.e.m. (40 vessel window) is overlaid. Inset bar graphs show mean \pm s.e.m. for each of the three vessel types. *** $P < 10^{-3}$, significantly different from baseline.

network was equal to its output. Such measurements were only possible in networks where all input and output vessels had a segment parallel to the focal plane; this requirement was achieved in two networks (Figures 5B and 5C). In these cases, we

confirmed that flux was essentially conserved during all three imaging periods within an error range of 5% ($n = 6$). As in the data with random sampling (Figure 5A, right panel), the integrated flux through penetrating arterioles was restored to baseline

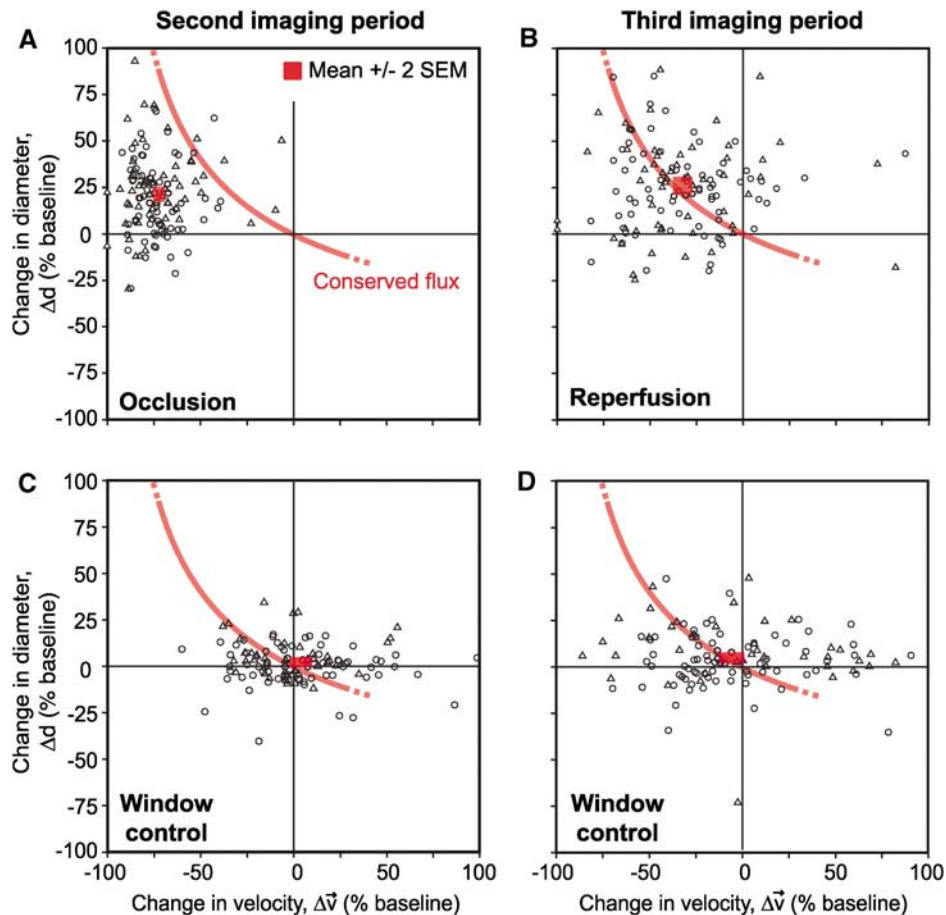


Figure 4 Vasodilation tracks RBC velocity to conserve flux during reperfusion. (**A** and **B**) Change in the lumen diameter plotted as a function of change in RBC velocity during the occlusion and reperfusion periods, respectively. The interface where RBC flux is conserved, based on Equation (2), is shown in red. All points on the curve indicate maintenance of baseline levels of flux; those to the left of the curve have substandard flux, whereas those to the right have enhanced flux. A red box, mean \pm 2 s.e.m., is the mean response over all vessels. During occlusion (**A**), the mean response is significantly different from the closest point on the line of conserved flux; $P < 10^{-3}$ (two-sided one sample *t*-test). In contrast, the mean response during reperfusion (**B**) is not significantly different from the line of conserved flux; $P > 0.05$ (two-sided one sample *t*-test). Data represents 131 small surface arterioles (triangles) and penetrating arterioles (circles) combined from 11 tMCAo experiments. Large surface arterioles were not included in this analysis. (**C** and **D**) Vasodynamic changes in Window control groups, i.e., cranial window with no vascular manipulation, showed no significant difference from the line of conserved flux in either the second or third period of imaging; $P > 0.05$ (two-sided one-sample *t*-test). For controls, each imaging period was maintained for the same time span as the tMCAo experimental group, i.e., 90 mins. Data represents 113 small surface arterioles and penetrating arterioles combined from 6 Window control experiments.

levels during reperfusion, whereas the total flux input to the network from large surface arterioles was reduced.

Reperfusion after Transient Middle Cerebral Artery Occlusion Relieves Hypoxia in Penumbral Cortex

To examine whether recovery of RBC flux to penetrating arterioles was consistent with tissue re-oxygenation, we tested for hypoxic tissue in the imaged region using pimonidazole accumulation as a probe of hypoxia (Takasawa *et al*, 2008). Consistent with an earlier study, pimonidazole injection during the period of occlusion led to heterogeneous staining of hypoxic cells throughout the MCA-supplied

territory (Figures 6A to 6D, left column) (Noto *et al*, 2006). Interestingly, blood vessels and the immediate neuropil surrounding the vessels appeared largely unlabeled in the cortex (Figure 6C, arrowheads). In contrast to occlusion, when pimonidazole was injected immediately after the onset of reperfusion, the dorsal cortex was largely unstained, suggesting homogeneous re-oxygenation of the postischemic tissue (Figures 6A to 6D, right column); we noted only sparse labeling of individual cells with neuronal morphology (Figure 6C, right panel inset). Importantly, even after reperfusion, areas within the lateral cortex often remained labeled (Figure 6B, right panel), which confirmed that this method was capable of detecting areas with poor reperfusion. Laser Doppler flowmetry was used to

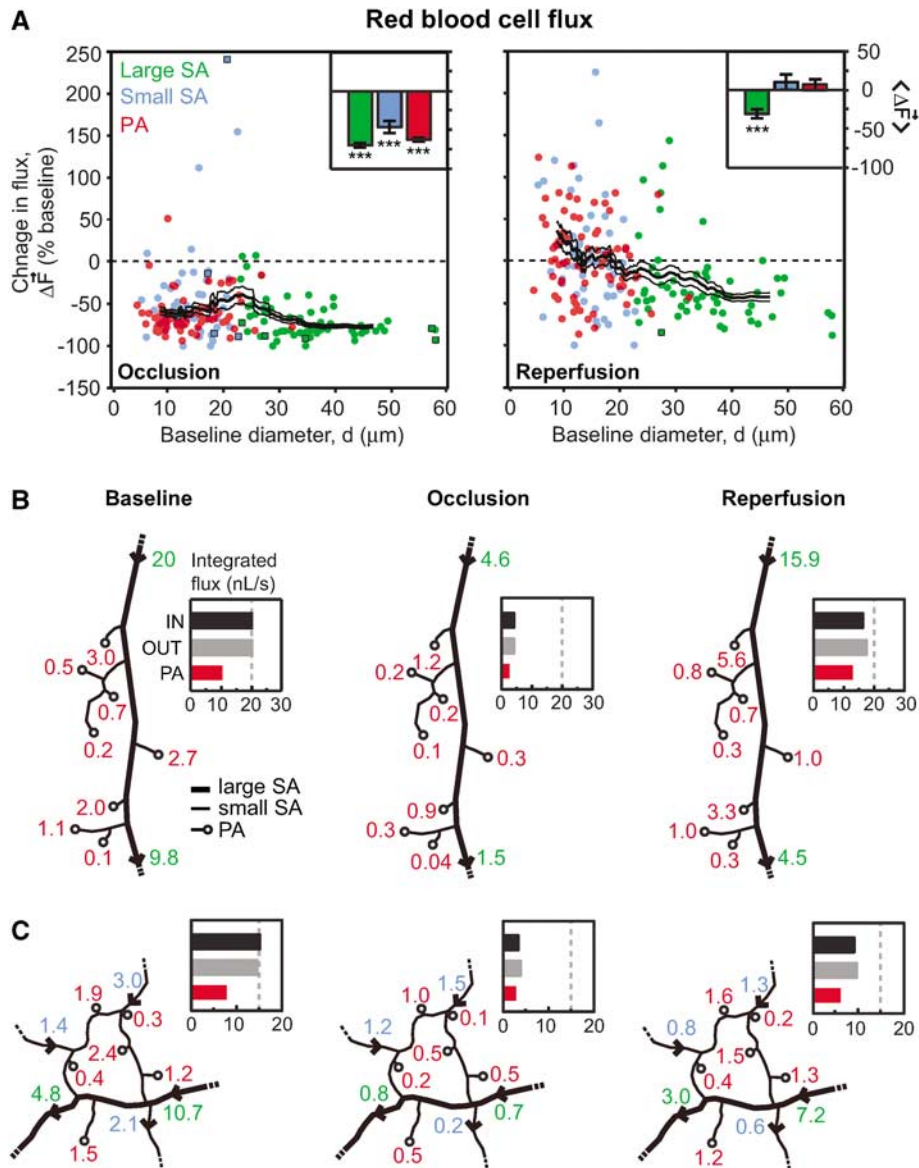


Figure 5 Change in RBC volume flux during tMCAo. **(A)** Change in RBC flux during occlusion and reperfusion plotted as a function of baseline diameter. Square data points represent arterioles with reversed flow with respect to baseline. A running average \pm s.e.m. (40 vessel window) is overlaid. Inset bar graphs show average change in flux \pm s.e.m. for each of the three vessel types. $***P < 10^{-3}$, significantly different from baseline. **(B and C)** In two separate experiments, cumulative flux entering and exiting an arteriole network was measured. Arterial traces with flux values, in nL/sec, are shown for each imaging period. A bar graph summarizes the net input (IN) and output (OUT) from the arteriole network during each period. Flux exiting only through penetrating arterioles (PA) is also shown.

ensure that a similar reduction in blood flow was achieved between occlusion- and reperfusion-injected groups, and that successful reperfusion was achieved in the latter group (data not shown). This result indicates that there are no poorly reperfused zones in the imaged region at surface and subsurface levels consistent with full reperfusion of penetrating arterioles.

Preserved Arteriole Reactivity to Postischemic Hyperemia and Hypercapnia

As a final control, we tested whether postischemic arterioles could constrict during an increase in blood

flow above baseline levels, that is, hyperemia. A preserved myogenic response to hyperemia would indicate an active compensatory mechanism for change in vessel diameter rather than a passive loss of smooth muscle tone. For this experiment, we used a variation of the stroke model that maintained unobstructed flow of the ipsilateral CCA during reperfusion (Longa *et al*, 1989). This approach generated a transient period of flow increase, on average peaking at $\sim 20\%$ above baseline levels within 10 mins after de-occlusion, and lasting up to 0.5 h, as measured by LDF (Figure 7A). The high variability during this hyperemic period was not conducive for accurate vasodynamic measurements;

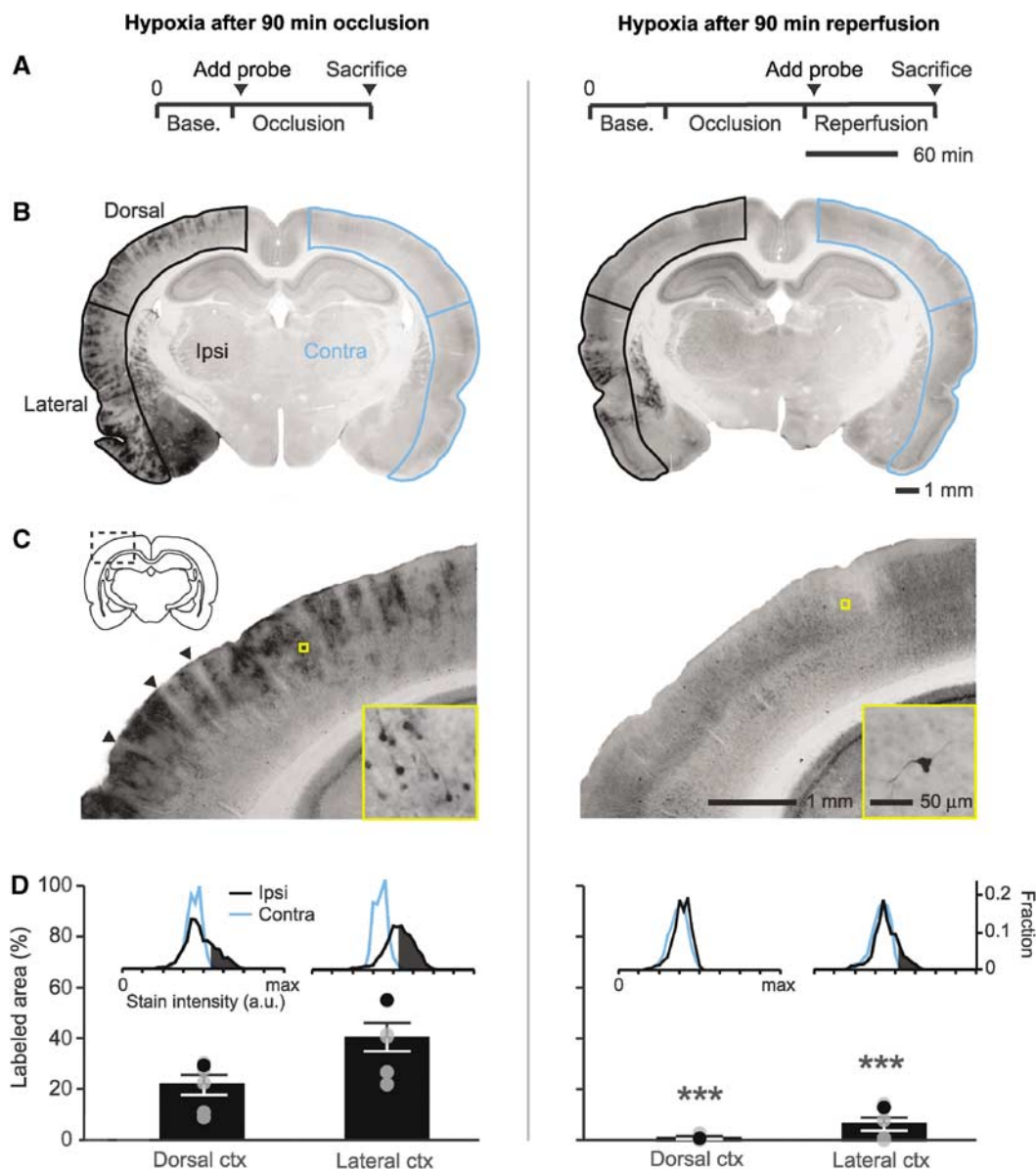


Figure 6 Absence of hypoxic tissue in the cortical penumbra during reperfusion. **(A)** Experimental timelines for the intra-arterial injection of pimonidazole, a marker of hypoxia. Probe circulation time between the two groups was equivalent, i.e., 90 mins. **(B)** Representative coronal images of pimonidazole labeling from animals injected during occlusion or reperfusion. Ipsilateral (black, ischemic side) and contralateral (blue) cortices were demarcated and separated into dorsal and lateral portions. **(C)** Magnified images of the dorsal cortex (dashed rectangle), with a further magnified view of stained cells (yellow square). Arrowheads indicate relatively unstained zones surrounding penetrating vessels. **(D)** Average labeled area \pm s.e.m. expressed as the percentage of total dorsal or lateral cortical area. Black points within the scatter plot represent the animal shown in the figure. Inset histograms illustrate the threshold setting used to differentiate positive staining in the ipsilateral cortex from background, defined as the lower 90% of the intensity histogram from the contralateral side (see also Materials and methods). $***P < 10^{-3}$, significantly different from the group injected at occlusion (unpaired *t*-test).

therefore, we analyzed arterioles measured between 0.5 h and 1.5 h after reperfusion onset when RBC velocity and diameter were stabilized.

We found that arterioles dilated by ischemia were capable of constricting in response to the postischemic hyperemic period (31 small surface arterioles and 42 penetrating arterioles over 4 animals) (Figures 7B to 7D); this is a result consistent with earlier studies (Pinard *et al*, 2002). Interestingly,

RBC flux after hyperemia was below baseline levels (Figure 7E), suggesting that vasoconstriction could be involved in postischemic hypoperfusion in this model. Finally, dilation could be re-induced by hypercapnia (10% CO₂ for 20 mins) during a fourth period of imaging (Figures 7B and 7D), leading to a significant increase in flux (Figure 7E). These data confirm that penetrating arterioles were capable of active bi-directional changes in diameter after stroke.

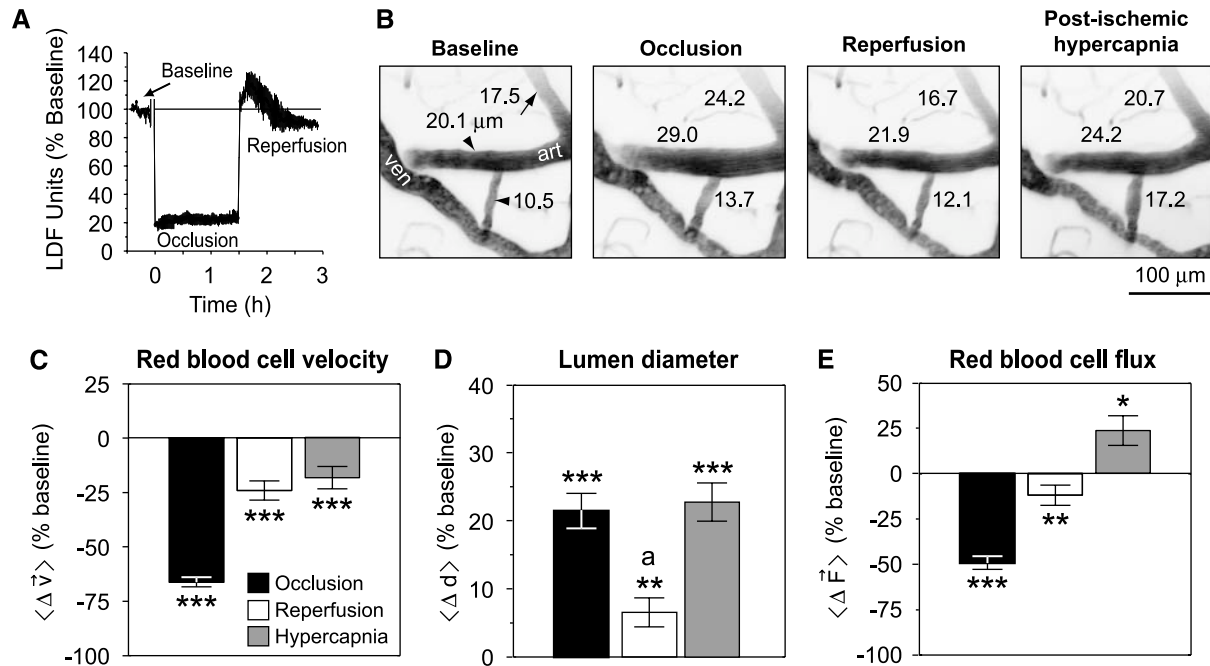


Figure 7 Active vascular responses to postischemic hyperemia and hypercapnia. **(A)** Laser Doppler flowmetry measurements reveal a period of hyperemia after reperfusion in the Longa model of tMCAo (Longa *et al*, 1989). Laser Doppler flowmetry data represent mean \pm s.e.m. from $n = 3$ animals. An approximately 10-min period during filament insertion was omitted from the trace. **(B)** Representative images of diameter changes for two penetrating arterioles (arrowheads) and a small surface arteriole (arrow) in response to occlusion, reperfusion, and hypercapnia. The images are maximal projections of 100 μm deep image stacks with 5 μm steps. **(C to E)** Average changes in measured vascular parameters for 73 small surface arterioles and penetrating arterioles from 4 tMCAo experiments. Data represent mean \pm s.e.m. *** $P < 10^{-3}$, ** $P < 0.01$, and * $P < 0.05$ significantly different from baseline, $^{\text{a}}P < 10^{-3}$, significantly different from diameter during occlusion and hypercapnia (paired t -test).

Discussion

To examine the homeostatic function of cerebral pial arterioles after ischemia, we measured RBC flux in networks of arterioles that overlie the cortical penumbra of focal stroke. Three major findings are highlighted, they are: (i) Although flow reversals and stalls occur in arterioles of the surface collateral network, they are not observed within penetrating arterioles. (ii) The change in flux of RBCs during ischemia cannot be predicted from the changes in their velocity or in the lumen diameter alone. (iii) Small diameter surface arterioles and penetrating arterioles are the main vasoreactive components of the pial arteriole network. In our paradigm, active dilation of small arterioles compensated for incomplete recovery of RBC velocity during reperfusion to enable the full recovery of RBC flux in penetrating arterioles.

Flow Pattern Changes in the Pial Network

Earlier studies characterized changes in the pattern of flow throughout arteriole networks in response to occlusion of the MCA (Schaffer *et al*, 2006), and with respect to peri-infarct depolarization (Pinard *et al*, 2002). In this study, these flow irregularities were mapped to specific arteriole networks by using vascular casts to define arteriole connectivity

beyond that observed through the imaging window (Figures 1A and 2). Our findings indicate that flow reversals and stalls serve in the redistribution of blood to ensure homogeneous supply of penetrating arterioles during low-flow conditions. Consistent with this design, penetrating arterioles neither reversed nor stalled at any point during focal stroke. Of the total measured surface arterioles, 72% resided within loop structures or were directly connected to ACA collaterals. Despite this large fraction, blood flow reversed or stalled in only 12% of the vessels. This suggests that the occurrence of flow shifts was not limited by arteriole connectivity, and that relatively few shifts were necessary to maintain homogeneous flow through penetrating arterioles during ischemia.

Determination of Red Blood Cell Flux in Pial Arterioles

The determination of RBC flux is an improvement in *in vivo* studies that evaluate blood flow on the basis of vessel diameter alone. In particular, the measurement of only one parameter can be misleading, as the velocity of RBCs and diameter of a vessel can vary independently, particularly during disturbances of blood flow. This difficulty was explicitly noted by Kontos (1989) and is supported by studies that show stroke-induced pial arteriole dilation alone is a poor

indicator of downstream flow to tissue (Pinard *et al*, 2002; Tasdemiroglu *et al*, 1992). Our results confirm that reliance on only a single indicator of blood flow provides an incomplete description of the vascular response to stroke. In the Koizumi tMCAo paradigm, RBC velocity alone suggests an incomplete recovery of blood flow during reperfusion (Figures 3A and 3C), whereas diameter measurements considered alone support persistent vasodilation and therefore increased flow (Figures 3B and 3D). The calculation of flux from these parameters (Equation (1)), however, showed that blood flow in fact recovered to baseline levels during reperfusion (Figure 5A).

One potential caveat of our methodology is that serum flow is not measured. Indeed, serum supplies both glucose and oxygen in ischemic states, in addition to other nutritional sources. By measuring arterio-venous transit times of a fluorescent dye, Rovainen *et al* (1993) found net serum flow to be on average three times faster than RBC flow. Serum flow may persist even when RBCs are stalled and may still represent a significant source of oxygen during ischemia (Villringer *et al*, 1994).

Preservation of Small Arteriole Reactivity in the Focal Stroke Penumbra

Our findings reveal that arteriole reactivity in the stroke penumbra remains intact and capable of modulating lumen diameter as a compensatory mechanism to conserve RBC flux at these time points of ischemia and reperfusion. By distinguishing between the differing sizes and types of pial arterioles, the primary locus of reactivity was shown to reside in small surface arterioles and penetrating arterioles. We confirmed that small arterioles ($< 23 \mu\text{m}$) were capable of constriction in response to transient hyperemia after stroke (Figures 7B and 7D), and thus did not become passively dilated owing to the loss of vascular tone. Although we did not evaluate the arteriole response over a wide autoregulatory curve (Kontos *et al*, 1978), these results nonetheless indicate that myogenic reactivity to increased flow is intact at the level of individual arterioles. Further, our findings with hypercapnic treatment (Figures 7B and 7D) are consistent with studies that show partial preservation of reactivity to CO_2 in the stroke penumbra (Jones *et al*, 1989). Finally, at a histologic level, parenchymal vessels within the penumbra did not bind pimonidazole during both occlusion and reperfusion periods, suggesting limited hypoxic damage (Figure 6C, left panel).

An open question is how net dilation of only smaller-diameter arterioles affects the pial network flow as a whole. We showed that total RBC flux into and out of these networks was conserved (Figures 5B and 5C). However, during reperfusion, the total flux available was reduced compared with baseline, consistent with incomplete recovery of flux in large surface arterioles, whereas penetrating arteriole flux returned to baseline (Figure 5B). Penetrating arterioles thus extracted a

larger proportion of the available blood from large supply vessels, perhaps causing a reduction in flow to watershed regions sourced by both the MCA and ACA (Momjian-Mayor and Baron, 2005). This may represent a form of cerebrovascular steal, where blood flow is intercepted from the hypoperfused ischemic focus by highly collateralized and reactive penumbral regions (Scremin, 1991). We suspect that unbalanced delivery of blood between the stroke penumbra and core may, in part, contribute to the poor re-oxygenation of the lateral cortex during reperfusion (Figure 6B, right panel).

What are the long-term consequences of ischemia on penetrating arteriole reactivity? Recent work by Cipolla and colleagues suggest that isolated penetrating lentulo-striate arterioles possess normal myogenic tone and reactivity 24 h after a 1-h period of transient and moderate ischemia (Cipolla and Bullinger, 2008). Interestingly, these arterioles exhibited compensatory alterations in nitric oxide and endothelial-derived hyperpolarizing factor signaling to maintain normal vascular function. In a related study, Ngai *et al* (2007) also found no effect on the cerebral penetrating arteriole tone 24 h after 1 to 2 h of transient ischemia, and further showed that conducted dilatatory responses along penetrating arterioles were augmented after stroke. These recent findings are in contrast to surface arterioles isolated from severely ischemic zones surrounding the proximal MCA, which lose tone even after 30 mins of ischemia as a result of structural damage to arteriole smooth muscle (Cipolla and Curry, 2002). Taken together with the results of this study, small surface arterioles and penetrating arterioles appear to be unique in their ability to adapt and maintain regulatory function after transient ischemia. Although the mechanisms that underlie this preferential resistance to ischemia remain to be defined, the preserved reactivity of penetrating arterioles will be a key determinant for improved recovery after stroke.

Acknowledgements

We thank Agnieszka Prechtel for assistance with immunohistochemistry, Christopher A. Rafie for assistance with fluorescent vascular casts, Anna Devor for surgical advice, and Jonathan Driscoll and Pablo Blinder for comments on the manuscript.

Disclosure

The authors state no conflict of interest.

References

- Bar T (1980) The vascular system of the cerebral cortex. *Adv Anat Embryol Cell Biol* 59:1–62
- Barfod C, Akgoren N, Fabricius M, Dirnagl U, Lauritzen M (1997) Laser-Doppler measurements of concentration and velocity of moving blood cells in rat cerebral circulation. *Acta Physiol Scand* 160:123–32

- Cipolla MJ, Bullinger LV (2008) Reactivity of brain parenchymal arterioles after ischemia and reperfusion. *Microcirculation* 15:495–501
- Cipolla MJ, Curry AB (2002) Middle cerebral artery function after stroke: the threshold duration of reperfusion for myogenic activity. *Stroke* 33:2094–9
- Cipolla MJ, Lessov N, Hammer ES, Curry AB (2001) Threshold duration of ischemia for myogenic tone in middle cerebral arteries: effect on vascular smooth muscle actin. *Stroke* 32:1658–64
- Cipolla MJ, Li R, Vitullo L (2004) Perivascular innervation of penetrating brain parenchymal arterioles. *J Cardiovasc Pharmacol* 44:1–8
- Devor A, Hillman EM, Tian P, Waeber C, Teng IC, Ruvinskaya L, Shalinsky MH, Zhu H, Haslinger RH, Narayanan SN, Ulbert I, Dunn AK, Lo EH, Rosen BR, Dale AM, Kleinfeld D, Boas DA (2008) Stimulus-induced changes in blood flow and 2-deoxyglucose uptake dissociate in ipsilateral somatosensory cortex. *J Neurosci* 28:14347–57
- Devor A, Tian P, Nishimura N, Teng IC, Hillman EM, Narayanan SN, Ulbert I, Boas DA, Kleinfeld D, Dale AM (2007) Suppressed neuronal activity and concurrent arteriolar vasoconstriction may explain negative blood oxygenation level-dependent signal[s]. *J Neurosci* 27:4452–9
- Dirnagl U, Pulsinelli W (1990) Autoregulation of cerebral blood flow in experimental focal brain ischemia. *J Cereb Blood Flow Metab* 10:327–36
- Dirnagl U, Villringer A, Einhaupl KM (1992) *In-vivo* confocal scanning laser microscopy of the cerebral microcirculation. *J Microsc* 165:147–57
- Eger II EI (1981) Isoflurane: a review. *Anesthesiology* 55:559–76
- Heistad DD, Kontos HA (eds) (1983) *Cerebral circulation*. Bethesda: American Physiological Society
- Iadecola C (1998) Cerebral circulatory dysregulation in ischemia. In: *Cerebrovascular disease: pathophysiology, diagnosis, and management* (Ginsberg MD, ed), Malden: Blackwell Publishing, 319–32
- Jones SC, Bose B, Furlan AJ, Friel HT, Easley KA, Meredith MP, Little JR (1989) CO₂ reactivity and heterogeneity of cerebral blood flow in ischemic, border zone, and normal cortex. *Am J Physiol* 257:H473–82
- Kleinfeld D, Friedman B, Lyden PD, Shih AY (2008) Targeted occlusion to surface and deep vessels in neocortex via linear and nonlinear optical absorption. In: *Animal models of acute neurological injuries* (Chen J, Xu Z, Xu X-M *et al*, eds), Totowa: The Humana Press Inc, 169–83
- Kleinfeld D, Mitra PP, Helmchen F, Denk W (1998) Fluctuations and stimulus-induced changes in blood flow observed in individual capillaries in layers 2 through 4 of rat neocortex. *Proc Natl Acad Sci USA* 95:15741–6
- Koizumi J, Yoshida Y, Nakazawa T, Ooneda G (1986) Experimental studies of ischemic brain edema: 1. A new experimental model of cerebral embolism in rats in which recirculation can be introduced in the ischemic area. *Jpn J Stroke* 8:1–8
- Kontos HA (1989) Validity of cerebral arterial blood flow calculations from velocity measurements. *Stroke* 20:1–3
- Kontos HA, Wei EP, Navari RM, Levasseur JE, Rosenblum WI, Patterson JIJ (1978) Responses of cerebral arteries and arterioles to acute hypotension and hypertension. *Am J Physiol* 234:H371–83
- Lipton P (1999) Ischemic cell death in brain neurons. *Physiol Rev* 79:1431–568
- Longa EZ, Weinstein PR, Carlson S, Cummins R (1989) Reversible middle cerebral artery occlusion without craniectomy in rats. *Stroke* 20:84–91
- Marshall RS (2004) The functional relevance of cerebral hemodynamics: why blood flow matters to the injured and recovering brain. *Curr Opin Neurol* 17:705–9
- Momjian-Mayor I, Baron JC (2005) The pathophysiology of watershed infarction in internal carotid artery disease: review of cerebral perfusion studies. *Stroke* 36:567–77
- Ngai AC, Nguyen TS, Meno JR, Britz GW (2007) Post-ischemic augmentation of conducted dilation in cerebral arterioles. *Stroke* 38:124–30
- Ngai AC, Winn HR (1996) Estimation of shear and flow rates in pial arterioles during somatosensory stimulation. *Am J Physiol* 270:H1712–7
- Nguyen Q-T, Tsai PS, Kleinfeld D (2006) MPScope: a versatile software suite for multiphoton microscopy. *J Neurosci Methods* 156:351–9
- Nishimura B, Schaffer CB, Friedman B, Lyden PD, Kleinfeld D (2007) Penetrating arterioles are a bottleneck in the perfusion of neocortex. *Proc Natl Acad Sci USA* 104:365–70
- Nishimura N, Schaffer CB, Friedman B, Tsai PS, Lyden PD, Kleinfeld D (2006) Targeted insult to individual subsurface cortical blood vessels using ultrashort laser pulses: three models of stroke. *Nat Methods* 3:99–108
- Noto T, Furuichi Y, Ishiye M, Matsuoka N, Aramori I, Mutoh S, Yanagihara T, Manabe N (2006) Temporal and topographic profiles of tissue hypoxia following transient focal cerebral ischemia in rats. *J Vet Med Sci* 68:803–7
- Paulson OB, Strandgaard S, Edvinsson L (1990) Cerebral autoregulation. *Cerebrovasc Brain Metab Rev* 2:161–92
- Pinard E, Nallet H, MacKenzie ET, Seylaz J, Roussel S (2002) Penumbra microcirculatory changes associated with peri-infarct depolarizations in the rat. *Stroke* 33:606–12
- Rovainen CM, Woolsey TA, Blocher NC, Wang D-B, Robinson OF (1993) Blood flow in single surface arterioles and venules on the mouse somatosensory cortex measured with videomicroscopy, fluorescent dextrans, nonoccluding fluorescent beads, and computer-assisted image analysis. *J Cereb Blood Flow Metab* 13:359–71
- Schaffer CB, Friedman B, Nishimura N, Schroeder LF, Tsai PS, Ebner FF, Lyden PD, Kleinfeld D (2006) Two-photon imaging of cortical surface microvessels reveals a robust redistribution in blood flow after vascular occlusion. *Public Library of Science Biology* 4:258–70
- Scremin OU (1991) Pharmacological control of the cerebral circulation. *Annu Rev Pharmacol Toxicol* 31:229–51
- Takasawa M, Moustafa RR, Baron JC (2008) Applications of nitroimidazole *in vivo* hypoxia imaging in ischemic stroke. *Stroke* 39:1629–37
- Tasdemiroglu E, Macfarlane R, Wei EP, Kontos HA, Moskowitz MA (1992) Pial vessel caliber and cerebral blood flow become dissociated during ischemia-reperfusion in cats. *Am J Physiol* 263:H533–6
- Tsai PS (2004) All-optical histology using two photon laser scanning microscopy and ablation with ultrashort pulses. Thesis (PhD). San Diego: University of California
- Tsai PS, Friedman B, Ifarraguerri AI, Thompson BD, Lev-Ram V, Schaffer CB, Xiong Q, Tsien RY, Squier JA,

- Kleinfeld D (2003) All-optical histology using ultrashort laser pulses. *Neuron* 39:27–41
- Tsai PS, Nishimura N, Yoder EJ, Dolnick EM, White GA, Kleinfeld D (2002) Principles, design, and construction of a two photon laser scanning microscope for *in vitro* and *in vivo* brain imaging. In: *In vivo optical imaging of brain function* (Frostig RD, ed), Boca Raton: CRC Press, 113–71
- Villringer A, Them A, Lindauer U, Einhaupl K, Dirnagl U (1994) Capillary perfusion of the rat brain cortex: an *in vivo* confocal microscopy study. *Circ Res* 75:55–62

Supplementary Information accompanies the paper on the Journal of Cerebral Blood Flow & Metabolism website (<http://www.nature.com/jcbfm>)